# An Optimal and Non-Linear Speed Control of Oscillating Water Column Wave Energy Plant with Wells Turbine and DFIG

Sunil Kumar Mishra*‡, Shubhi Purwar*, Nand Kishor*

* Department of Electrical Engineering, Motilal Nehru National Institute of Technology, Allahabad-211004, India

(hariomsunil88@gmail.com, shubhi@mnnit.ac.in, nandkishor@mnnit.ac.in)

‡ Corresponding Author; Sunil Kumar Mishra, Tel: +91 9208291117,

*Received: 09.04.2016 Accepted: 19.06.2016*

**Abstract-** This paper presents controller scheme to maximize the turbine output power and thereby improve the efficiency in oscillating water column (OWC) wave power plant equipped with Wells turbine and doubly fed induction generator (DFIG). The scheme is based on flow coefficient estimation and controller design for tracking of rotational speed. Initially, a linear reference tracking (LRT) approach is applied to achieve the maximized output power by establishing a linear relationship between reference rotational speed and input pressure drop. This follows implementation of fuzzy theory based maximum power point tracking (FMPPT) approach to provide the optimal speed reference. Then, a backstepping (BS) controller is designed to track reference rotational speed of DFIG so as to improve the output power. The BS controller is derived using Lyapunov stability theorem which ensures the stability of the overall closed loop system. The advantages of the proposed control scheme over conventional PI control and the uncontrolled system is demonstrated for regular waves and irregular waves. Finally, the FMPPT-BS control approach has been validated with JONSWAP irregular wave model.

**Keywords** Backstepping control, DFIG, fuzzy MPPT, oscillating water column, Wells turbine.

## 1. Introduction

The community world-wide is in search for clean and renewable energy resources mainly due to (i) rapid increase in demand of energy all over the world (ii) global warming as a result of excessive use of fossil fuels for power generation. Apart from solar, wind and nuclear energy resources, oceans have immense energy potential in the form of waves, tides etc. and over the last years many technologies have been developed to tap the ocean wave energy [1].

The main challenges of ocean wave energy have been the design difficulties and the higher financial risks involved. But in recent years, ocean wave power has received a decent attention of research community. The impetus of wave energy research has increased substantially. Several projects covering various aspects of ocean wave power plants are being investigated all over the globe [2-6]. Among the approaches reported in literature, the oscillating water column (OWC) design is one of the widely considered methodologies for ocean wave energy conversion [7-9].

One of the key research topics of OWC ocean wave energy converter is the design of appropriate control schemes for efficient operation under uncertain ocean wave conditions. The uncontrolled electrical power is difficult to be connected to the grid as well as the conventional control strategies may not be perfect for efficient operation. Thus, wave power generation requires advanced control approaches. Some important control strategies can be categorized into rotational speed control, air flow control, output power control and fault-ride-through mechanisms [10-16].A detailed survey on control methods can be found in [17].

Fuzzy logic theory has been applied for maximum energy extraction of renewable energy sources such as photovoltaic cells, wind energy systems etc. [18-20]. The fuzzy logic approach is preferred over conventional maximum power extraction methods due to advances in computer technology, materials and power electronics.

In recent times, the backstepping (BS) control strategy has become popular among the research community and the reason being the systematic control law design approach [21]. The BS controller is based on recursive approach where state variables can be utilized as pseudo-control inputs for next subsystems of the plant to be controlled. At each step, a new pseudo-control input is derived from previous pseudo-control stages and the stability of each stage is ensured by virtue of a Lyapunov function. At the last stage, a control law is derived by adding the Lyapunov functions of all the

pseudo-control stages. Several studies [22-25] reveal that this control strategy is very effective for highly nonlinear systems like wind turbine-DFIG systems as compared to conventional PI based controls and other nonlinear control strategies, e.g. sliding mode (SM) control [26].

The present study deals with rotor speed control of Wells turbine-doubly fed induction generator (DFIG) system with the objective of (i) avoiding the stalling behaviour of Wells turbine (ii) maximizing the output power and efficiency of the OWC wave power plant. Initially, this presents a linear reference tracking (LRT) approach to maximize the power by obtaining a linear expression between the reference rotor speed and the average input pressure. Thereafter, to overcome the limitations of the LRT approach, a cascaded control strategy wherein the outer loop that generates the optimal reference of rotor speed and the inner loop for tracking of rotor speed is discussed. The outer loop consists of a fuzzy based maximum power point tracking (FMPPT), whereas the inner loop is equipped with a BS controller. The stability of rotor speed and rotor side flux states has been guaranteed using Lyapunov stability theory. The proposed control scheme is demonstrated on various input pressure drop conditions inside the OWC chamber. This simulation study takes into account system behaviour under different regular and irregular sea wave conditions. The JONSWAP (Joint North Sea Wave Project) wave spectrum [27] is used to generate the irregular wave profiles for validating the proposed control scheme. All the controlled cases are compared with the conventional PI based control [11] and uncontrolled cases.

The rest of the paper is arranged under the following headings: **Section 2** describes the fundamentals of ocean waves and the structure of OWC wave power plant equipped with turbine-generator module. The control problems of OWC plant are stated in **Section 3**. The control design approach has been discussed in **Section 4**. Simulation results with different sea wave scenarios for controlled and uncontrolled cases are discussed in **Section5**. The concluding remarks on proposed control scheme are given in **Section 6**.

## 2. Description of OWC Wave Energy Plant

The basic structure of OWC as shown in Fig.1 (a) includes a hollow structure which is partially submerged in water and upper part of the column is filled with air [28]. The bottom of the column is open to sea to receive the sea water waves and the top of the structure is mounted with a Well turbine coupled to a DFIG. The stator side of the DFIG is directly connected to the grid, and 30% of the rated power is transferred back to the rotor side with help of two back to back AC/DC/AC convertors. These convertors are used to control the variable speed operation of DFIG which makes the DFIG operation more efficient and robust as compared to squirrel cage machine or wound rotor machine with external rotor resistances. As the wave strikes the column, rise and fall of water level inside the chamber takes place according to the wave period. As a result, air pressure in the chamber oscillates. The bidirectional flow of air drives the air turbine-DFIG system. Finally, the ocean wave energy gets converted into electrical energy.

### *2.1. Ocean Waves- Introduction*

Wind with very high velocity or the storm striking the sea surface at a faraway distance from coastal line, results into the swell of sea water. The swells take the shape of waves which are called ocean waves or sea waves. These swells accompanied by very large height and intensity are capable of reaching coastal area. The wind speed profiles are of variable nature at different places because of the geography of the earth and as well as its dependence on the pressure difference generated by the solar energy due to highly uneven distribution of solar radiations. Thus, the variable wind pattern creates the variable sea water wave pattern. The potential of the wave power stored in the oceans is uneven throughout the world [29].

There are many theoretical studies available on study related to the characteristics of ocean waves [30, 31]. The highly nonlinear and uncertain nature of the real sea waves makes the theoretical study very difficult. Thus, the ocean wave theories generally consider the sea waves as linear and then nonlinearities are added as the perturbation to the ideal linear wave. The simplified form of an ocean wave can be seen in Fig. 1(b). The highest and lowest peaks of the wave are called crest and trough respectively. The wave height ($H$) is defined as the difference between crest and trough. The distance between the sea bed and still water level (SWL) is called sea depth ($D$). The distance between two consecutive troughs or crests is known as the wavelength ($\lambda$) of the wave.

The energy of a wave per unit length is defined by [30]:

$$\mathrm{E} = \frac{\rho_w.\mathrm{g}.H^2\,\lambda}{8}\ (J/m) \tag{1}$$

Therefore, the wave energy per unit area also known as specific energy of waves can be given as:

$$\bar{E} = \frac{E}{\lambda} = \frac{\rho_w.g.H^2}{8}\ (J/m^2) \tag{2}$$

Where, $\rho_w$ is the water density ($Kg/m^3$) and $g$ is the gravitational constant ($9.81\ m/s^2$).

The propagation speed of a wave is defined as:

$$C = \frac{\lambda}{T}\ (m/s) \tag{3}$$

Where, $T$ is the wave period ($s$).

The rate at which wave energy propagates is directly dependent on the group velocity of the wave. The group velocity is given by:

$$C_g = n.C\ (m/s) \tag{4}$$

Where, $C_g$ is the celerity (wave front velocity) ($m/s$), $n$ is the constant determined by:

$$n = \frac{1}{2}\left[1 + \frac{4\pi D/\lambda}{\sinh(4\pi D/\lambda)}\right] \tag{5}$$

The wave resources are generally defined by the wave power stored in per meter of the wave front. Therefore, the wave front power can be described as:

$$P_{wavefront} = n.C.\bar{E} = C_g.\bar{E} \quad (6)$$

$$P_{wavefront} = \frac{\rho_w.g.H^2.\lambda}{16T}\left[1+\frac{4\pi D/\lambda}{\sinh(4\pi D/\lambda)}\right] \quad (7)$$

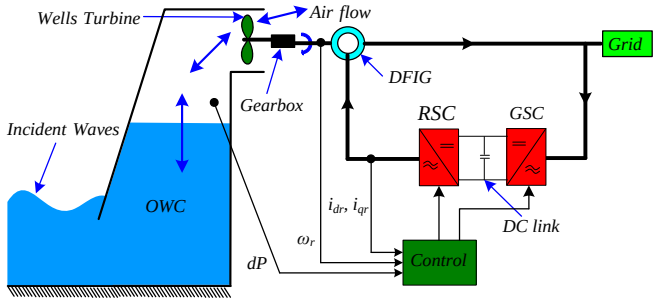


(a) Ocean wave energy plant

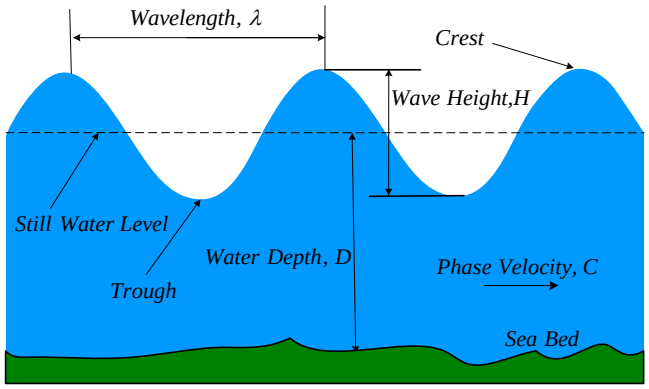


(b) Ocean wave

**Fig. 1** Schematic representation of ocean wave power plant and characteristics of ocean waves

### *2.2. Wells Air Turbine*

The Wells turbine works due to variable pressure oscillations creating the bidirectional air flow inside the OWC chamber [32]. The air flow is converted into unidirectional rotatory motion. The mathematical equations of power coefficient ($C_a$) and torque coefficient ($C_t$) of the Wells turbine are given as [33]:

$$C_a = (dP.a_t)/(k_t.(v_x^2+(r\omega_t)^2)) \quad (8)$$

$$C_t = T_t/(k_t.r.(v_x^2+(r\omega_t)^2)) \quad (9)$$

Where, $dP$ is the differential pressure drop (N/m$^2$), $a_t$ is the cross sectional area (m$^2$), $v_x$ is the air-flow velocity (m/s), $\omega_t$ is the turbine angular velocity (rad/s), $r$ is the mean radius (m), $k_t$ is the turbine constant (kg/m) given by:

$$k_t = \rho.b.l.n_t/2 \quad (10)$$

Where, $l$ is the blade chord length, $b$ is the blade height, $n_t$ is the number of blades, $\rho$ is the air density ($Kg/m^3$).

The turbine torque ($T_t$) and turbine power ($P_t$) is:

$$T_t = dP.\frac{C_t}{C_a}.r.a_t \quad (11)$$

$$P_t = T_t.\omega_t \quad (12)$$

The power coefficient ($C_a$) and torque coefficient ($C_t$) of the Wells turbine depends on the flow coefficient ($\phi$) which is one of the very important parameter of the Wells turbine given by:

$$\phi = v_x.(r\omega_t)^{-1} \quad (13)$$

The turbine efficiency ($\eta_t$) is given by:

$$\eta_t = \frac{P_t}{P_{in}} = \frac{T_t.\omega_t}{dP.Q} = \frac{C_t}{C_a.\phi} \quad (14)$$

Where, Q is the air flow rate i.e. $Q=v_x.a_t$ (m$^3$/s).

Further, the average efficiency [34] of Wells turbine ($\bar{\eta}$) can be expressed as:

$$\bar{\eta} = \left(\frac{1}{T}\int_0^T (T_t.\omega_t)dt\right)\Big/\left(\frac{1}{T}\int_0^T (dP.Q)dt\right) \quad (15)$$

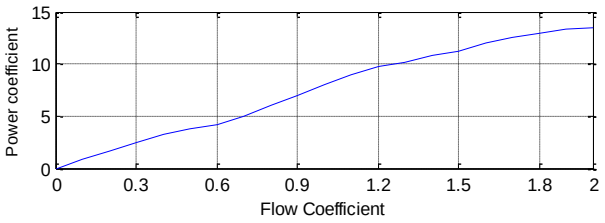


(a) Power coefficient versus flow coefficient

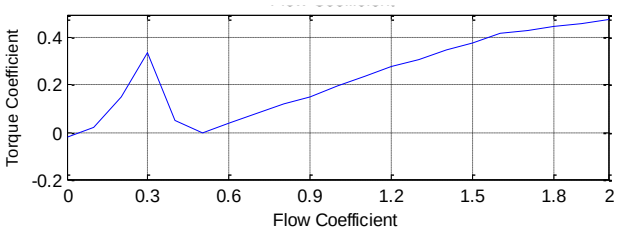


(b) Torque coefficient versus flow coefficient

**Fig. 2** Wells turbine characteristics [14]

The variation in power coefficient and torque coefficient of the Wells turbine are shown in Figs. 2(a) & (b). The flow of turbine is directly proportional to the air flow velocity as given in Eqn. (13). Thus, the increase in air flow velocity increases the flow coefficient which in turn increases the torque coefficient ($C_t$) until the value of flow coefficient reaches 0.3. However, for flow coefficient greater than 0.3 the $C_t$ value decreases and leads to the stalling phenomenon of Wells turbine. As a result, the turbine efficiency decreases tremendously which in turn generates very low output power and would be analysed in **section 3**.

### *2.3. Doubly Fed Induction Generator*

The study considers the d-q equivalent dynamic model of the generator because of the advantage that all the sinusoidal variables in stationary frame appear as DC

quantities referred to the synchronous rotating frame [35]. The mathematical equations of DFIG in terms of stator and rotor flux states for d- and q-axis respectively are given as:

$$\frac{d}{dt}\psi_{ds} = -\frac{R_s L_r}{K}\psi_{ds} + \omega_e \psi_{qs} + \frac{R_s L_m}{K}\psi_{dr} + V_{ds} \quad (16)$$

$$\frac{d}{dt}\psi_{qs} = -\omega_e \psi_{ds} - \frac{R_s L_r}{K}\psi_{qs} + \frac{R_s L_m}{K}\psi_{qr} + V_{qs} \quad (17)$$

$$\frac{d}{dt}\psi_{dr} = \frac{R_r L_m}{K}\psi_{ds} - \frac{R_r L_s}{K}\psi_{dr} - (\omega_r - \omega_e)\psi_{qr} + V_{dr} \quad (18)$$

$$\frac{d}{dt}\psi_{qr} = \frac{R_r L_m}{K}\psi_{qs} + (\omega_r - \omega_e)\psi_{dr} - \frac{R_r L_s}{K}\psi_{qr} + V_{qr} \quad (19)$$

The expressions for the electromagnetic torque and the power generated are:

$$T_e = M(\psi_{qs}\psi_{dr} - \psi_{ds}\psi_{qr}) \quad (20)$$

$$P_g = T_e.\omega_r \quad (21)$$

The relationship between various currents and flux linkages of the generator are given by:

$$\left.\begin{array}{ll} \psi_{qs} = L_s i_{qs} + L_m i_{qr}; & \psi_{ds} = L_s i_{ds} + L_m i_{dr} \\ \psi_{qr} = L_r i_{qr} + L_m i_{qs}; & \psi_{dr} = L_r i_{dr} + L_m i_{ds} \\ L_s = L_{ls} + L_m; & L_r = L_{lr} + L_m \end{array}\right\} \quad (22)$$

Where, $M = \frac{3}{2}\left(\frac{p}{2}\right)\left(\frac{L_m}{K}\right)$; $K = L_s L_r - L_m^2$; $R_s$, $R_r$: Stator and rotor resistance (Ω); $L_s$, $L_r$: Total stator and rotor inductance (H); $L_{ls}$, $L_{lr}$: Stator and rotor leakage inductance (H); $L_m$: Magnetizing inductance (H); $v_{qs}$, $v_{qr}$: q-axis stator and rotor voltage (V); $v_{ds}$, $v_{dr}$: d-axis stator and rotor voltage (V); $i_{qs}$, $i_{qr}$: q-axis stator and rotor current (A); $i_{ds}$, $i_{dr}$: d-axis stator and rotor current (A); $\psi_{qs}$, $\psi_{qr}$: q-axis stator and rotor flux (Wb); $\psi_{ds}$, $\psi_{dr}$: d-axis stator and rotor flux (Wb); $\omega_e$, $\omega_r$: Stator supply frequency and rotor speed (rad/s); $p$: Number of poles of the generator; $T_e$: Electro-magnetic torque (N-m).

The coupling relationship between the Wells turbine and DFIG is given as:

$$J\dot{\omega}_r + F\omega_r = g_b.T_t - T_e \quad (23)$$

Where, $g_b$ is the gear box ratio, i.e. $g_b=\omega_t/\omega_r$, $J$ is the moment of inertia of turbo-generator system (kg m$^2$), $F$ is the friction coefficient (kg m$^2$ s$^{-1}$), $T_t$ is the torque produced by the turbine (N-m).

## 3. Control Problem Statement

The performance analysis of the turbine over a wide range of pressure drop for uncontrolled condition is given in Table 1.The flow coefficient of the Wells turbine increases with the increase in input pressure level. As soon as the flow coefficient surpasses the threshold limit, the turbine starts stalling and the torque coefficient (see Fig. 2(b)) reduces [14]. Subsequently, the turbine efficiency and average mechanical power also decreases. Thus, the control problem can be divided into two stages; selection of optimal reference speed and rotational speed control of turbine according to variations in pressure drop.

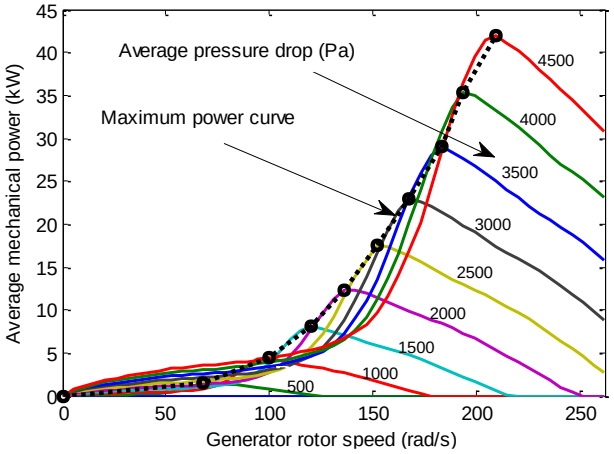


**Fig. 3** Power-speed curve for OWC wave power plant with different input pressure conditions

### *3.1. Selection of Optimal Reference Speed*

The variation in characteristic between average mechanical power and rotor speed for different input pressure conditions is shown in Fig. 3. The average mechanical power attains peak value at a specified rotor speed for a particular input pressure. The rotor speed corresponding to maximum mechanical power is considered as optimal reference value to run the turbine. The selection of optimal reference speed for wide range of pressure drops is necessary to avoid the turbine stalling. Thus, a MPPT tracking scheme is developed to obtain the optimal reference speed that ensures the maximum output power operation.

### *3.2. Rotational Speed Control*

The PI based control [14] and sliding mode control [26] for OWC wave power plants have been discussed in the past. The PI controller being a linear one, when implemented to highly nonlinear system like OWC plant in closed loop system may lead to the instability under uncertain waves. Though, the sliding mode controller ensures the asymptotic stability of the closed loop system but also suffers with the well-known chattering phenomenon. Thus, the robust and nonlinear control strategy for OWC wave power plants is developed which satisfies maximum power operation and ensures the stability of the closed loop system.

## 4. Design of Control Schemes for OWC Wave Energy Plant

The control structure of complete OWC wave power plant is illustrated in Fig. 4(a). The differential pressure drop and rotor speed serve as input variables to the MPPT block whose output is the optimal reference speed. The rotor speed is compared with the optimal reference speed and their error is as input to the controller. The essential feature of the BS control is the design of a control law $U$ so that the actual rotor speed precisely tracks the reference speed for various ranges of input pressure drop.

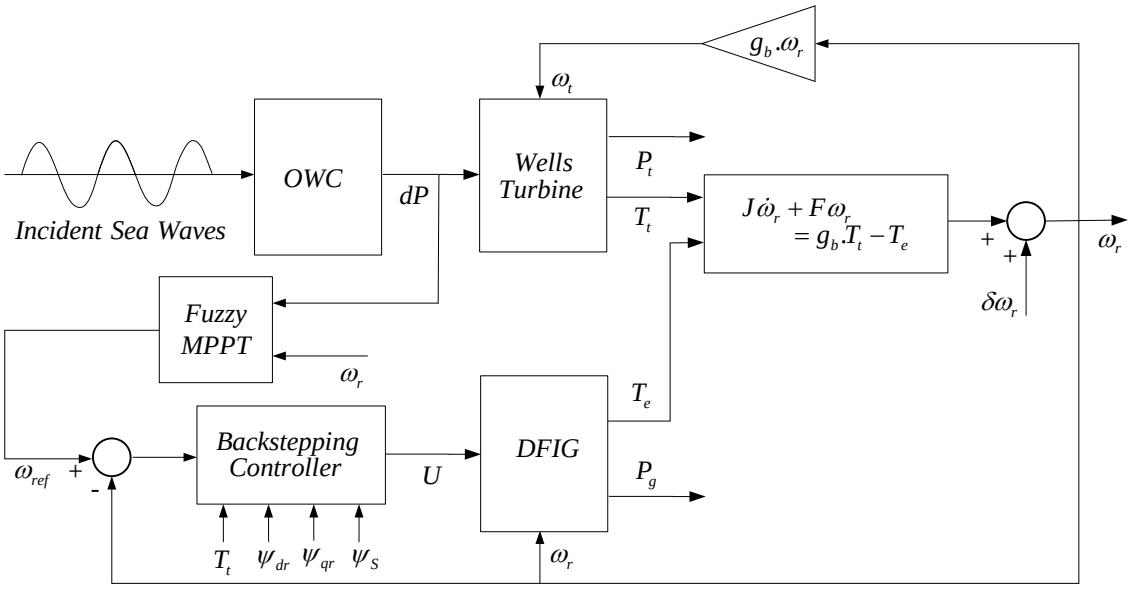


(a) Fuzzy MPPT tracking based backstepping control

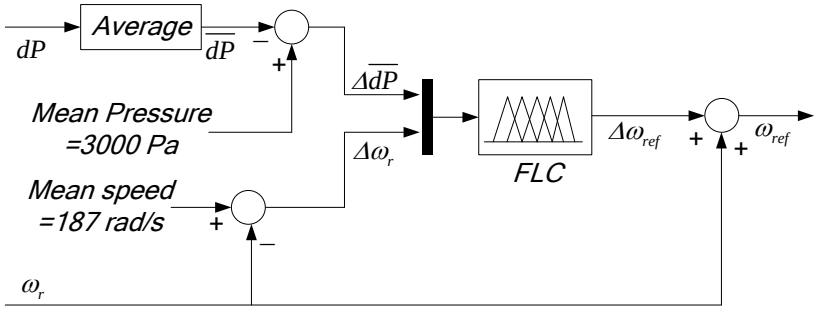


(b) FMPPT tracking

**Fig. 4** Block representation of proposed rotational speed control scheme for OWC wave power plant

**Table 1.** Turbine performance for uncontrolled case

| Average Pressure (Pa) | Flow Coefficient | Average Turbine Efficiency (%) | Average Mechanical Power (kW) |
|---|---|---|---|
| 1500 | 0-0.1830 | 24.94 | 5.56 |
| 2000 | 0-0.2375 | 28.88 | 10.90 |
| 2500 | 0-0.2881 | 31.22 | 17.26 |
| 3000 | 0-0.3374 | 29.14 | 19.54 |
| 3500 | 0-0.3847 | 24.32 | 17.06 |
| 4000 | 0-0.4348 | 20.51 | 13.89 |
| 4500 | 0-0.4835 | 18.10 | 11.85 |

The output of BS controller is $U = [V_{dr}\ V_{qr}]^T$ which is converted from *dq* to *abc* transformation to generate gate pulses for rotor side converter (RSC) using pulse width modulation (PWM) approach. The modelling of the rotor side converter and grid side converter (GSC) is not discussed as the present study mainly focuses on control scheme. Next, subsections follows on the implementation of tracking scheme and backstepping control design. These are discussed under the following subheadings as (i) the linear reference tracking (LRT) method (ii) the FMPPT method and (iii) the BS controller design.

### *4.1. Estimation of Flow Coefficient-Linear Reference Tracking Scheme*

As discussed above (Fig. 3), under normal operating conditions, the average value of input pressure should lie in the range [1500, 4500] Pa and the rotational speed range should be [157, 217] rad/s. In this range, the characteristic can be considered as linear. Thus, by choosing the minimum and maximum points for pressure and speed, a linear equation can be established for reference speed that directly

depends on the input pressure. A linear equation between two points ($x_1$, $y_1$) and ($x_2$, $y_2$) can be expressed as:

$$y - y_1 = \frac{y_2 - y_1}{x_2 - x_1}\,(x - x_1) \tag{24}$$

For this case, $x = \overline{dP}$, $y = \omega_{ref}$; $x_1$=1500 Pa, $y_1$=157 rad/s and $x_2$=4500 Pa, $y_2$=217 rad/s. Therefore(24), becomes:

$$\omega_{ref} - 157 = \frac{217 - 157}{4500 - 1500}\,(\overline{dP} - 1500) \tag{25}$$

After solving the Eqn. (25), the final expression of LRT for rotor reference speed in terms of input pressure can be written as:

$$\omega_{ref} = 2 \times 10^{-2}\,\overline{dP} + 127 \tag{26}$$

Eqn. (26) provides the expression for the linear tracking of reference speed depending on the average value of input pressure but it may not be as effective as required for all the conditions because the curve (Fig. 3) is inherently nonlinear. Thus, a nonlinear MPPT approach is discussed in the next section to take into account the nonlinear nature of the said MPPT curve.

### 4.2. Estimation of Flow Coefficient- Fuzzy based MPPT (FMMPT) Scheme

In this section, the fuzzy logic theory is applied to achieve optimum speed for maximum power extraction. The proposed fuzzy logic approach consists of two input variables; input pressure deviation ($\Delta\overline{dP}$) and rotor speed deviation ($\Delta\omega_r$) and output variable as the reference speed deviation ($\Delta\omega_{ref}$) that is added to the actual rotor speed in order to generate the optimal speed reference ($\omega_{ref}$) as shown in Fig. 4(b). The mean value for speed and pressure are 187rad/s and 3000Pa respectively. Therefore, the expressions for input pressure deviation ($\Delta\overline{dP}$) and rotor speed deviation ($\Delta\omega_r$) can be written as:

$$\left.\begin{aligned} \Delta\overline{dP} &= (3000 - \overline{dP})\ \text{Pa} \\ \Delta\omega_r &= (187 - \omega_r)\ \text{rad/s} \end{aligned}\right\} \tag{27}$$

**Table 2** Fuzzy rules

| $\Delta\omega_r$ | $\Delta\overline{dP}$ | | | | | | |
|---|---|---|---|---|---|---|---|
| | **LN** | **MN** | **SN** | **Z** | **SP** | **MP** | **LP** |
| **LN** | Z | Z | Z | MP | LP | LP | LP |
| **MN** | SN | SN | SN | SP | MP | LP | LP |
| **SN** | MN | MN | MN | Z | SP | MP | LP |
| **Z** | LN | LN | LN | SN | Z | SP | MP |
| **SP** | LN | LN | LN | MN | SN | Z | SP |
| **MP** | LN | LN | LN | LN | MN | SN | Z |
| **LP** | LN | LN | LN | LN | LN | MN | SN |

The functional structure consists of fuzzification, fuzzy rules and defuzzification. For, fuzzification, the triangular membership functions with seven fuzzy subsets has been considered. The variables lie in the range ±1500 Pa for input pressure deviation and ±30 rad/s for both rotor speed deviation and reference speed deviation. The centre of gravity defuzzification method has been applied for calculating the output of the FMPPT block. The fuzzy rules for input and output variables are expressed in terms of linguistic variables as LN (large negative), MN (means negative), SN (small negative), Z (zero), SP (small positive), MP (means positive), and LP (large positive) as given in Table 2. The control rules generate the optimal reference speed to maximize the power. After obtaining the expression for optimal reference speed, the approach for obtaining the BS control law is formulated as explained in the next section.

### 4.3. The Backstepping Controller Design and its Stability

The most common control related feature of DFIG is the field oriented control having d-axis of the stator frame aligned along the stator flux linkage i.e. $\psi_{ds}=\psi_s$ and $\psi_{qs}=0$. As the stator is connected to the grid, the effect of stator resistance is very small and thus the stator flux $\psi_s$ can be treated as constant. From Eqn. (16), the expression for $V_{ds}$ can be given as:

$$V_{ds} = \frac{R_s L_r}{K}\psi_S - \frac{R_s L_m}{K}\psi_{dr} \tag{28}$$

If the stator resistance is neglected or if $\psi_{dr} = (L_r / L_m)\psi_S$ in Eqn. (28) then in both the cases $V_{ds}$ becomes zero.

Here, the $\psi_{dr}$ can be used as one of the pseudo-control input for next stage which may be expressed as:

$$\psi_{dref} = \frac{L_r}{L_m}\psi_S \tag{29}$$

Similarly, the expression for $V_{qs}$ can be obtained from the Eqn. (17) as $V_{qs} = \omega_e \psi_S = V_S$. Therefore, the stator side grid voltage in terms of dq dynamics is given by:

$$[V_{ds}\ \ V_{qs}]^T = [0\ \ V_S]^T \tag{30}$$

Also the changed expression for electromagnetic torque ($T_e$) from Eqn. (20) can be written as:

$$T_e = -M\psi_{qr}\psi_S \tag{31}$$

Therefore, by substituting the Eqn. (31) into the Eqn. (23), the expression for $\dot{\omega}_r$ becomes:

$$\dot{\omega}_r = \frac{g_b}{J}\,T_t - \frac{F}{J}\,\omega_r + \frac{M}{J}\psi_{qr}\,\psi_S \tag{32}$$

Now, in the design of backstepping control scheme, the error between the reference rotor speed and actual rotor speed is given by:

$$e_1 = \omega_{ref} - \omega_r \tag{33}$$

The first derivative of Eqn. (33) is:

$$\dot{e}_1 = \dot{\omega}_{ref} - \dot{\omega}_r \tag{34}$$

On substituting the $\dot{\omega}_r$ from the Eqn. (32) into Eqn. (34), the error derivative term $\dot{e}_1$ becomes:

$$\dot{e}_1 = \dot{\omega}_{ref} - \frac{g_b}{J}\ T_t + \frac{F}{J}\ \omega_r - \frac{M}{J}\psi_{qr}\ \psi_S \tag{35}$$

To ensure that $e_1 \to 0$ as $t \to \infty$, a positive definite function also called as Lyapunov function is defined as:

$$V_1 = \frac{1}{2}e_1^2 \tag{36}$$

The derivative of the Eqn. (36) is $\dot{V}_1 = e_1\dot{e}_1$ that implies:

$$\left.\begin{aligned}\dot{V}_1 = -K_1e_1^2 + e_1(K_1e_1 + \dot{\omega}_{ref} - \frac{g_b}{J}\ T_t \\ + \frac{F}{J}\ \omega_r - \frac{M}{J}\psi_{qr}\ \psi_S)\end{aligned}\right\} \tag{37}$$

Where, $K_1$ is a constant greater than zero.

To make $\dot{V}_1$ a negative definite quantity, the $\psi_{qr}$ can be chosen as the pseudo-control input for next stage. Therefore:

$$\psi_{qref} = \frac{J}{M\psi_S}(K_1e_1 + \dot{\omega}_{ref} - \frac{g_b}{J}\ T_t + \frac{F}{J}\ \omega_r) \tag{38}$$

Thus, the $\dot{V}_1$ becomes as:

$$\dot{V}_1 = -K_1e_1^2 \le 0 \tag{39}$$

Now, Eqns. (29) and (38) would work as the pseudo-control input for next stage and the error dynamics for rotor flux states have been chosen as:

$$\left.\begin{aligned}e_2 = \psi_{dref} - \psi_{dr} \\ e_3 = \psi_{qref} - \psi_{qr}\end{aligned}\right\} \tag{40}$$

Taking the first derivative of Eqn. (40):

$$\left.\begin{aligned}\dot{e}_2 = \dot{\psi}_{dref} - \dot{\psi}_{dr} \\ \dot{e}_3 = \dot{\psi}_{qref} - \dot{\psi}_{qr}\end{aligned}\right\} \tag{41}$$

and putting the Eqns. (18) and (19) into Eqn. (41), the error derivatives can be expressed as:

$$\left.\begin{aligned}\dot{e}_2 = \dot{\psi}_{dref} - \frac{R_rL_m}{K}\psi_S + \frac{R_rL_s}{K}\psi_{dr} + (\omega_r - \omega_e)\psi_{qr} - V_{dr} \\ \dot{e}_3 = \dot{\psi}_{qref} - (\omega_r - \omega_e)\psi_{dr} + \frac{R_rL_s}{K}\psi_{qr} - V_{qr}\end{aligned}\right\} \tag{42}$$

Again, to ensure that all the error components $e_1, e_2, e_3 \to 0$ as $t \to \infty$, again a Lyapunov function has been defined as:

$$V = \frac{1}{2}e_1^2 + \frac{1}{2}e_2^2 + \frac{1}{2}e_3^2 \tag{43}$$

The first derivative of Eqn. (43) results into

$$\dot{V} = e_1\dot{e}_1 + e_2\dot{e}_2 + e_3\dot{e}_3 \tag{44}$$

and again putting the Eqns. (39) and (42) into the Eqn. (44), the final expression for $\dot{V}$ can be written as:

$$\left.\begin{aligned}\dot{V} = -K_1e_1^2 - K_2e_2^2 - K_3e_3^2 \\ + e_2\{K_2e_2 + \dot{\psi}_{dref} - \frac{R_rL_m}{K}\psi_S \\ + \frac{R_rL_s}{K}\psi_{dr} + (\omega_r - \omega_e)\psi_{qr} - V_{dr} \\ + e_3\{K_3e_3 + \dot{\psi}_{qref} - (\omega_r - \omega_e)\psi_{dr} \\ + \frac{R_rL_s}{K}\psi_{qr} - V_{qr}\}\end{aligned}\right\} \tag{45}$$

Therefore, the $\dot{V}$ can be made negative definite by choosing the $V_{dr}$ and $V_{qr}$ such that:

$$\left.\begin{aligned}V_{dr} = K_2e_2 + \dot{\psi}_{dref} - \frac{R_rL_m}{K}\psi_S + \frac{R_rL_s}{K}\psi_{dr} + (\omega_r - \omega_e)\psi_{qr} \\ V_{qr} = K_3e_3 + \dot{\psi}_{qref} - (\omega_r - \omega_e)\psi_{dr} + \frac{R_rL_s}{K}\psi_{qr}\end{aligned}\right\} \tag{46}$$

The $\dot{V}$ can be written as:

$$\dot{V} = -K_1e_1^2 - K_2e_2^2 - K_3e_3^2 \le 0 \tag{47}$$

Hence, the Eqn. (46) gives the final feedback backstepping control law U by ensuring the stability of all the states involved and the finalized control law $U$ is:

$$U = \begin{pmatrix} K_2e_2 + \dot{\psi}_{dref} - \frac{R_rL_m}{K}\psi_S + \frac{R_rL_s}{K}\psi_{dr} + (\omega_r - \omega_e)\psi_{qr} \\ K_3e_3 + \dot{\psi}_{qref} - (\omega_r - \omega_e)\psi_{dr} + \frac{R_rL_s}{K}\psi_{qr} \end{pmatrix} \tag{48}$$

The control law as developed above is used in the simulation studies and presented in the next section.

## 5. Simulation Results and Discussion

In this section, the simulation study is presented for wide range of pressure drops or sea wave conditions. The MATLAB/Simulink model of OWC power plant is developed. The power rating of DFIG is taken as 55 kW and the limit on rotor control voltages is set as ($V_{qr}$ and $V_{dr}$) is ±100 volts. Other parameters of turbine, generator and backstepping controller are given in Table 3.

Input pressure drop for regular waves is considered as [16, 23]:

$$dP = \frac{A}{2}(1 + sin(0.2\pi t))\ Pa \tag{49}$$

Where, A is the peak pressure drop and the average quantity is $\overline{dP} = A/2\ Pa$.

Input pressure drop for irregular waves considered as:

$$dP = [\frac{A+\delta A}{2}(1+sin(0.2\pi t))+\delta dP]\ Pa \qquad (50)$$

Where, $\delta A$ is the disturbance to the peak pressure drop whereas $\delta dP$ is uncertainty added to the overall pressure drop.

**Table 3** Turbine, generator and controller parameters

| Turbine | Generator | Controller |
|---|---|---|
| $n$=8 | $p$=4 | $K_1$=10 |
| $k_t$ =0.7079 | $R_s$=0.0181 | $K_2$=10 |
| $r$=0.7285 | $L_{ls}$=0.13 | $K_3$=50 |
| $a_t$=1.1763 | $L_m$=7.413 | |
| $b$=0.4 | $R_r$=0.0334 | |
| $l$=0.38 | $L_{lr}$=0.16 | |
| $g_b$ =1:2 | $f$=50Hz | |
| $J$=50 | $V_s$=390/√3 V | |

It is important to mention that the dynamic variation given by Eqns. (49) & (50) do not exactly represent the real sea waves but their linearized forms. These pressure profiles (Eqns. 49 & 50) are helpful in understanding the basic dynamics of the overall system and parameters such as peak pressure, average pressure and time period of pressure oscillations can be used to formulate the control strategies for wave power plants. Fig. 5 illustrates the variation in regular and irregular wave pressure drop.

*5.1. Regular Waves*

The flow coefficients being estimated by above discussed techniques, OWC wave power plant is simulated for wide range of regular wave pressure drops. The computed average mechanical power and efficiency is given in Table 4. The maximum values of flow coefficient always remain below 0.3 for all pressure values that fulfil the primary objective of avoiding stalling behaviour of the Wells turbine. The said table clearly indicates the advantages of FMPPT method over LRT estimation. Increased turbine efficiency is obtained using FMPPT for estimation of flow coefficient. Due to space restriction in manuscript, the simulation results only on the FMPPT-BS control method and its comparison with FMPPT-PI control/uncontrolled (without control) are discussed. Fig. 6 shows the OWC plant performance for regular waves. The flow coefficient of Wells turbine remains within the permissible range (i.e. 0-0.3) for both the control schemes as shown in Fig. 6(a). The rotational speed tracking using FMPPT-BS control is superior to both the FMPPT-PI control and without control case (Fig. 6(b)). The performance of required control effort in case of the FMPPT-BS control is more cost effective than the FMPPT-PI, since the latter approach undergoes a transient response which is within the desired limit of ±100 volts. This is illustrated in Fig. 6(c)-(d). The difference between the FMPPT-BS and FMPPT-PI controlled system/uncontrolled system can be seen in Fig. 7 in terms of electrical power generated. The electrical output power for FMPPT-BS (Fig. 7(c)) control is found to be much higher than both uncontrolled case (Fig. 7(a)) and FMPPT-PI control (Fig. 7(b)).

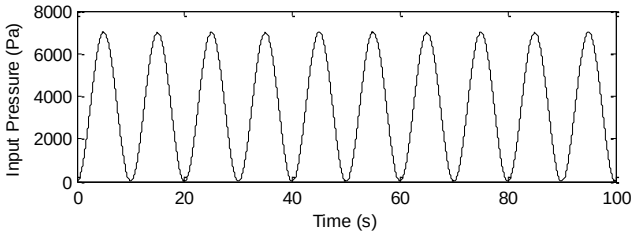


a) Regular Wave

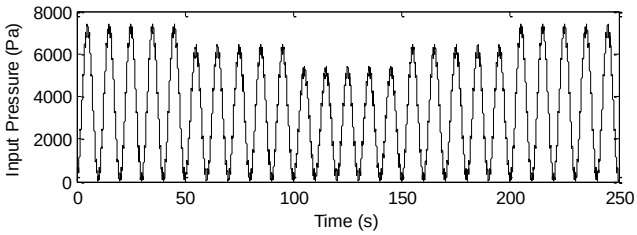


(b) Irregular Wave

**Fig. 5** Input pressures

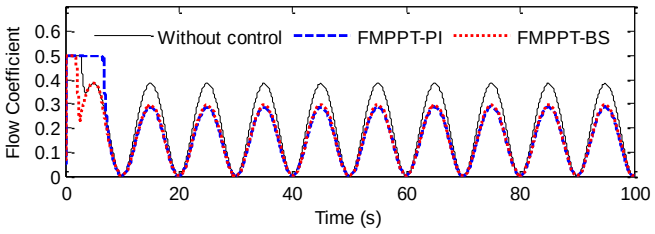


(a) Flow coefficient

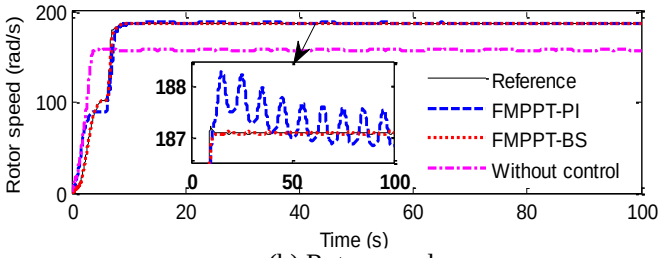


(b) Rotor speed

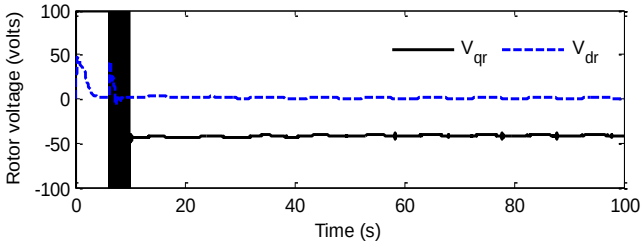


(c) FMPPT-PI control efforts

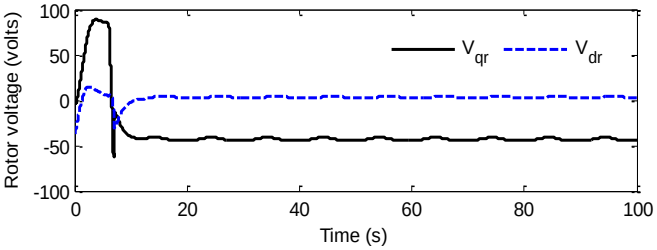


(d) FMPPT-BS control efforts

**Fig. 6** OWC plant performance for regular waves

**Table 4** The OWC plant performance with the LRT and the FMPPT

| Average pressure drop (Pa) | Flow coefficient estimation | | Average turbine efficiency (%) | | Average mechanical power (kW) | |
|---|---|---|---|---|---|---|
| | LRT | FMPPT | LRT | FMPPT | LRT | FMPPT |
| 1500 | 0-0.1840 | 0-0.1840 | 24.94 | 24.94 | 5.56 | 5.56 |
| 2000 | 0-0.2150 | 0-0.2400 | 27.20 | 28.91 | 9.88 | 10.90 |
| 2500 | 0-0.2370 | 0-0.2923 | 28.70 | 31.20 | 15.10 | 17.80 |
| 3000 | 0-0.2530 | 0-0.2781 | 29.60 | 30.72 | 20.86 | 22.16 |
| 3500 | 0-0.2640 | 0-0.2890 | 30.14 | 31.10 | 27.08 | 28.49 |
| 4000 | 0-0.2724 | 0-0.2960 | 30.49 | 31.31 | 33.71 | 35.21 |
| 4500 | 0-0.2780 | 0-0.2999 | 30.70 | 31.42 | 40.71 | 42.26 |

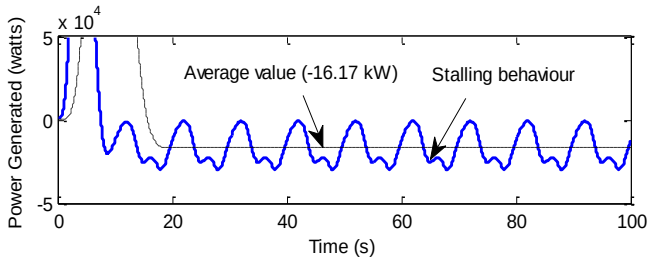


(a) Without control

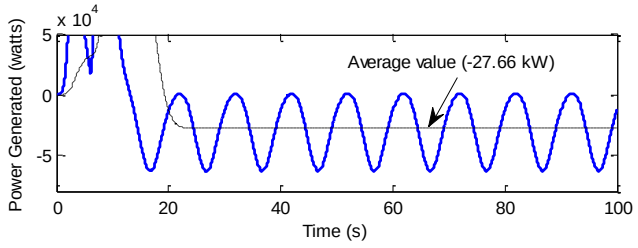


(b) FMPPT-PI control

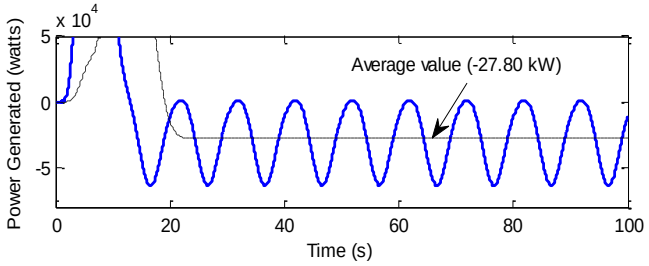


(c) FMPPT-BS control

**Fig. 7** Electrical power generated for regular waves

*5.2. Irregular Waves*

Next, the pressure behaviour of irregular waves which is characterized close to realistic sea is considered. The flow coefficient is forced to remain within the permissible range even under uncertain conditions of pressure drops as observed in Fig. 8(a).The corresponding variation in rotor speed achieved by two controllers has been shown in Fig. 8(b). As observed, FMPPT-BS control scheme successfully tracks the reference rotational speed as specified against the variations in pressure drops. The rotor voltage parameters undergo transient at the onset of input pressure change as indicated in Fig. 8(c). Further the required control effort by FMPPT-BS scheme as shown in Fig. 8(d) does not have undue transient unlike FMPPT-PI scheme.

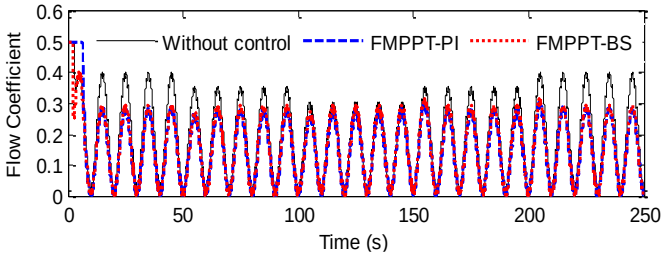


(a) Flow coefficient

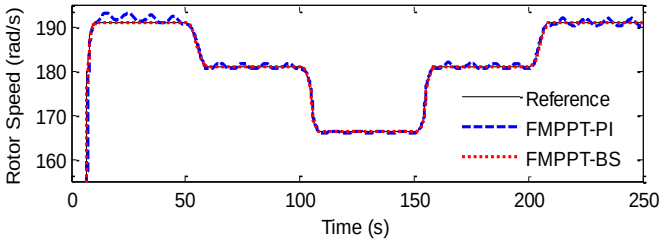


(b) Rotor speed

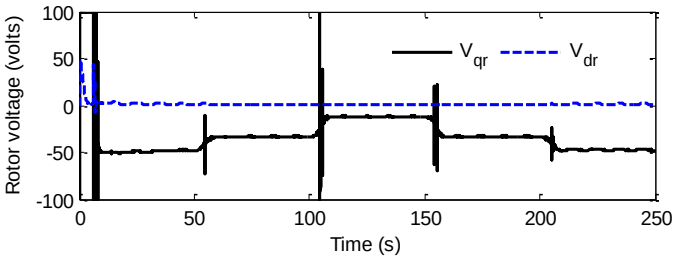


(c) FMPPT-PI control efforts

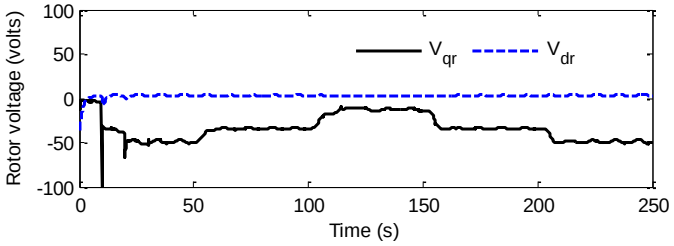


(d) FMPPT-BS control efforts

**Fig. 8** OWC plant performance for irregular waves

*5.3. JONSWAP Irregular Wave Model*

Now, the proposed FMPPT-BS control strategy is validated on JONSWAP irregular wave model using WAFO (Wave Analysis for Fatigue and Oceanography) toolbox [36, 37]. The JONSWAP wave spectrum is obtained from real sea wave measurements to characterize the ocean waves for the North Sea (Atlantic Ocean). As shown in Fig. 9(a), the wave energy spectrum is distributed over 0.35 rad/s to 1.5 rad/s, having highest energy component at 0.574 rad/s. This wave model is based on stochastic modelling and thus generates unseen wave patterns. Fig. 9(b) shows the pressure profile generated from JONSWAP spectrum. There is very large variation in differential pressure of OWC chamber reflecting the real nature of ocean wave energy. The performance of the FMPPT-BS and PI control technique is shown in Fig. 10 (a)-(b) in which the actual rotor speed tracks the reference very precisely. Also, the control voltages remain in the limit as shown in Fig. 10 (c)-(d).

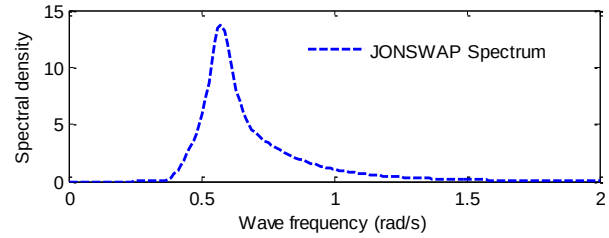


(a) JONSWAP wave spectrum

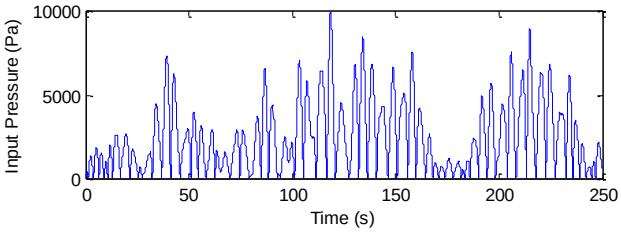


(b) Input pressure

**Fig. 9** JONSWAP irregular wave model

The quantitative performance comparison of FMPPT-BS and FMPPT-PI controllers using an integral square error (ISE) is given in Table 5. This further proves the efficacy of proposed FMPPT-BS control as the ISE values in this scheme remain lower than the FMPPT-PI control.

**Table 5** ISE performance for different wave profiles

| **Wave profile** | $ISE = \int_0^\infty e_1^2(t)\,dt$ | |
|---|---|---|
| | **FMPPT-BS** | **FMPPT-PI** |
| **Regular** | 927.4 | 989.4 |
| **Irregular** | 929.2 | 982.3 |
| **JONSWAP** | 950.8 | 966.7 |

## 6. Conclusion

In this work, the simulation studies have been carried out for OWC wave power plant to maximize its output power. In order to estimate the flow coefficient under various pressure drop conditions, linear reference tracking and fuzzy MPPT approaches were applied. Further, the backstepping control scheme was suggested in the controller design to track the rotational speed for various conditions. A comparatively higher turbine efficiency has been achieved using fuzzy MPPT with the BS controller. The performance of designed controller was compared with conventional PI type controller. The fuzzy MPPT-BS controller scheme performed satisfactorily in tracking of optimum reference rotational speed for regular waves and irregular waves. Also, the required control effort remained in the desired limit without undue transients. Finally, the proposed controller was also validated with JONSWAP spectrum based irregular wave model. The simulation results demonstrated that the proposed control scheme performed effectively under realistic sea conditions.

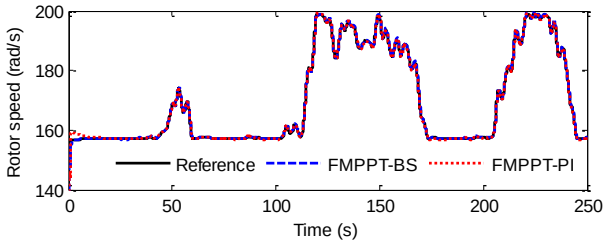


(a) Rotor speed

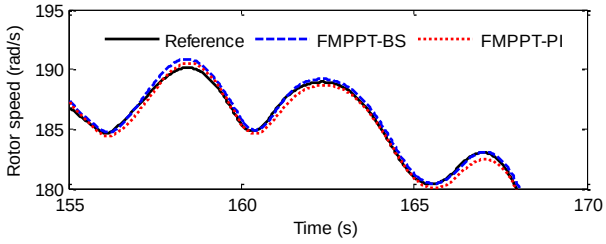


(b) Zoomed version of 10(a)

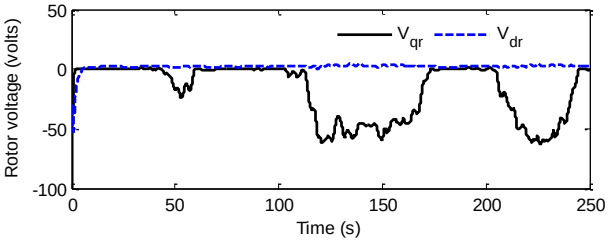


(c) FMPPT-BS control efforts

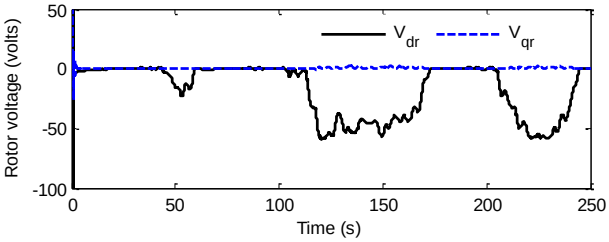


(d) FMPPT-PI control efforts

**Fig. 10** Performance of OWC wave power plant for JONSWAP irregular wave model

## References

[1] B. Czech, P. Bauer, "Wave energy convertor concepts: design challenges and classifications", IEEE Industrial Electronics Magazine, Vol. 6, No. 2, pp. 4-16, 2012.

[2] A. Clement, P. McCullenc, A. Falcão et al., "Wave energy in Europe: current status and perspectives", Renewable and Sustainable Energy Reviews, Vol. 6, pp. 405–431, 2002.

[3] K. Burman, A. Walker, "Ocean energy technology overview", The U.S. Department of Energy and the Office of Energy Efficiency and Renewable Energy, pp. 1-30, 2009.

[4] S. C. Parkinson, K. Dragoonb, G. Reikardc et al., "Integrating ocean wave energy at large-scales: A study of the US Pacific Northwest", Renewable Energy, Vol. 76, pp. 551-559, 2015.

[5] V. S. Kumar, T. R. Anoop, "Wave energy resource assessment for the Indian shelf seas", Renewable Energy, Vol. 76, pp. 212-219, 2015.

[6] K. Gunn, C. S. Williams, "Quantifying the global wave power resource", Renewable Energy, Vol. 44, pp. 296-304, 2012.

[7] A. F. O. Falcao, J. C. C. Henriques, "Oscillating-water-column wave energy converters and air turbines: A review", Renewable Energy, Vol. 85, pp. 1391-1424, 2016.

[8] J. F. Kelly, W. M. D. Wright, W. Sheng, "Implementation and Verification of a Wave-to-Wire Model of an Oscillating Water Column With Impulse Turbine", IEEE Transaction on Sustainable Energy, Vol. 7, No. 2, pp. 546-553, 2016.

[9] N. Delmonte, D. Barater, F. Giuliani, "Review of Oscillating Water Column Converters", IEEE Transactions on Industry Applications, Vol. 52, No. 2, pp. 1698-1710, 2016.

[10] M. A. Ormaza, M. A. Goitia, I. G. Hernandez, "Wells turbine Control in Wave Power Generation Plants", IEEE International Electric Machines and Drives Conference, May 2009, pp. 177-182.

[11] P. A. P. Justino, A. F. O. Falcão, "Rotational Speed Control of an OWC Wave Power Plant", Journal of Offshore Mechanics and Arctic Engineering, Vol. 121, No. 2, pp. 65-70, 1999.

[12] A. F. O. Falcão, L. C. Vieira, P. A. P. Justino et al., "By-Pass Air-Valve Control of an OWC Wave Power Plant", Journal of Offshore Mechanics and Arctic Engineering, Vol. 125, pp. 205-210, 2003.

[13] A. F. O. Falcão, P. A. P. Justino, "OWC wave energy devices with air flow control", Ocean Engineering, Vol. 26, pp. 1275–1295, 1999.

[14] M. Amundarain, M. Alberdi, A. J. Garrido, et al., "Modeling and Simulation of Wave Energy Generation Plants: Output Power Control", IEEE Transactions on Industrial Electronics, Vol. 58, No. 1, pp. 105-117, 2011.

[15] M. Amundarain, M. Alberdi, A. J. Garrido, et al., "Neural rotational speed control for wave energy converters", International Journal of Control, Vol. 84, No. 2, pp. 293–309, 2011.

[16] M. Alberdi, M. Amundarain, A. J. Garrido, et al., "Fault-Ride-Through Capability of Oscillating-Water-Column-Based Wave-Power-Generation Plants Equipped With Doubly Fed Induction Generator and Airflow Control", IEEE Transactions on Industrial Electronics, Vol. 58, No. 5, pp. 1501-1517, 2011.

[17] Y. Hong, R. Watersa, C. Boström et al., "Review on electrical control strategies for wave energy converting systems", Renewable and Sustainable Energy Reviews, Vol. 31, pp. 329–342, 2014.

[18] M. M. Algazar, H. AL-monier, H. Abd EL-halim, et al., "Maximum power point tracking using fuzzy logic control", Electrical Power and Energy Systems, Vol. 39, pp. 21–28, 2012.

[19] S. Abdeddaim, A. Betka, "Optimal tracking and robust power control of the DFIG wind turbine", Electrical Power and Energy Systems, Vol. 49, pp. 234–42, 2013.

[20] M. Azzouz, A.-l. Elshafei, H. Emara, "Evaluation of fuzzy-based maximum power-tracking in wind energy conversion systems", IET Renewable Power Generation, Vol. 5, No. 6, pp. 422–430, 2011.

[21] H. K. Khalil, Nonlinear Systems, Prentice Hall, 1996.

[22] G. D. Wang, R. J. Wai, Y. Liao, "Design of backstepping power control for grid-side converter of voltage source converter-based high-voltage dc wind power generation system", IET Renewable Power Generation, Vol. 7, No. 2, pp. 118–133, 2013.

[23] M. Loucif, , A. Boumediene, A. Mechernene, "Backstepping Control of Double Fed Induction Generator Driven by Wind Turbine", Proc. of the 3rd International Conference on Systems and Control, Algiers, Algeria, October 2013, pp. 153-158.

[24] S. Rajendran, D. Jena, "Backstepping sliding mode control of a variable speed wind turbine for power optimization", Journal of Modern Power Systems and Clean Energy, pp. 1-9, 2015.

[25] B. Bossoufi, M. Karim, A. Lagrioui, et al., "Observer backstepping control of DFIG-Generators for wind turbines variable-speed: FPGA-based implementation", Renewable Energy, Vol. 81, pp. 903-917, 2015.

[26] A. J. Garrido, I. Garrido, M. Amundarain, et al., "Sliding-Mode Control of Wave Power Generation Plants", IEEE Transactions on Industry Applications, Vol. 48, No. 6, pp. 2372-2381, 2012.

[27] K. Hasselmann, T. Barnett, E. Buows, et al., "Measurements of wind-wave growth and swell decay during the Joint North Sea Wave Project",.Deutschen Hydrografischen Zeitschrift, Vol. 12, pp. 9–95, 1973.

[28] J. C. C. Henriques, R. P. F. Gomes, L. M. C. Gato et al., "Testing and control of a power take-off system for an oscillating water-column wave energy converter", Renewable Energy, Vol. 85, pp. 714-724, 2016.

[29] L. Rodrigues, "Wave power conversion systems for electrical energy production", International Conference on Renewable Energies and Power Quality, Santander, March 2008.

[30] I. R. Young, "Wind Generated Ocean Waves', Ocean Engineering", Vol. 2, pp. 1-288, 1999.

[31] R. Bhattacharyya, M. E. McCormick, "Wave Energy Conversion", Ocean Engineering, Vol. 6, No. 1, pp. 1-187, 2003.

[32] A. F. O Falcão, J. C. C. Henriques, L. M. C. Gato, et al., "Air turbine choice and optimization for floating oscillating-water-column wave energy converter", Ocean Engineering, Vol. 75, pp. 148–156, 2014.

[33] V. Jayashankar, K. Udayakumar, B. Karthikeyan, et al., "Maximizing Power Output from a Wave Energy Plant", IEEE Power Engineering Society Winter Meeting, Vol. 3, pp. 1796-1801, 2000.

[34] T. Setoguchi, S. Santhakumar, M. Takao et al., "A modified Wells turbine for wave energy conversion", Renewable Energy, Vol. 28, pp. 79–91, 2003.

[35] B. K. Bose, Modern Power Electronics and AC Drives, Prentice Hall, 2002.

[36] P. A. Brodtkorb, G. Lindgren, I. Rychlik, et al., "WAFO-a Matlab Toolbox for Analysis of Random Waves and Loads", The 10th International Offshore and Polar Engineering Conference, USA, May 2000.

[37] D. Ramirez, J. P. Bartolome, S. Martinez, et al., "Emulation of an OWC Ocean Energy Plant With PMSG and Irregular Wave Model", IEEE Transactions on Sustainable Energy, Vol. 6, pp. 1515-1523, 2015.